Communication

Measurements and Analysis of Radio Propagation at 28 GHz in Vegetated Areas of Typical Residential Environments

Junghoon Ko, Sooyoung Hur, Yun-Seok Noh, Kuyeon Whang, Jeongho Park, Dong-Jo Park, and Dong-Ho Cho

***Abstract*— This communication presents foliage channel measurements at 28 GHz using a directional channel sounder. The measurements were conducted in vegetated areas of typical residential environments in Daejeon, South Korea. We first propose a pattern matching algorithm that allows us to overcome the angle resolution of a directional antenna and to estimate a more accurate receiving angle. Then propagation paths received from the vegetation and the surrounding buildings are classified and their power ratios are analyzed. Furthermore, foliage attenuation was determined from the measurement data according to the foliage depth, and appropriate models based on the modified exponential decay (MED) model and the maximum attenuation (MA) model are presented. In addition, the effect of foliage attenuation on seasonal variation is studied. These results will be useful for predicting path losses through the vegetated areas at 28 GHz by modeling the foliage loss as an additional path loss term. Finally, spatial–temporal channel characteristics in a vegetated environment were statistically analyzed including delay spread, coherence bandwidth, and angular spreads.**

***Index Terms*— 28 GHz, foliage, millimeter-wave (mm-wave), pattern matching, vegetation.**

I. Introduction

In recent years, the millimeter-wave (mm-wave) frequency band, which can utilize a wide bandwidth, has been attracting attention. In particular, the utilization of the mm-wave band is expected to solve the problem of limited spectrum resources below 6 GHz and enable beam-based communications through a large number of antennas. Accordingly, much research have been conducted to analyze the channel characteristics of the mm-wave band using directional channel sounders [1]–[3]. Vegetation is an inherent factor in most outdoor urban and suburban areas. The current standard does not take into account the effects of the foliage attenuation and assumes that the existing measurement results include these effects. However, in general, the attenuation due to vegetation in the mm-wave bands is more pronounced than in the conventional bands below 6 GHz [4], even though the anticipated tendency for the attenuation to increase with signal frequency is not always evident. One reason for higher attenuation in the mm-wave frequency is that the absorption phenomenon becomes more prominent, as the signal frequency increases. Another reason is related to the signal wavelength; the amount of signals scattered in other directions than the forward scattering direction also increases leading to a reduced signal level of the penetrating components, because the signal wavelength becomes comparable with the size of leaves and smaller branches presented in the canopy. Therefore, knowledge of the vegetation effects in a communication link in a residential environment can have a great influence on the system performance.

Many studies have been done to understand the foliage effects in the mm-wave bands and can be generally divided into analytical approaches and experimental approaches. Theoretical models are determined by mathematical formulations and describe physical propagation phenomena effectively. These analytical approaches, however, require numerical approximations for obtaining meaningful solutions due to their complex properties. In other words, they should be able to rigorously describe the electromagnetic information of the vegetation (leaves, trunk, branches, and so on). In [5], a numerical algorithm based on the radiative energy transfer (RET) theory was presented to calculate the foliage attenuation for mm-wave bands, and a comparison with scattering measurements at 75 GHz was shown. A ray-based model for scattering by vegetation has been developed and implemented in a preexistent ray-tracing tool and an empirical model in [6]. A simple ray-tracing-based model for single trees was presented and compared with a discretized RET approach in [7].

On the other hand, empirical models are represented by simple exponential equations, whose model structures and parameters can be obtained from channel measurements. These experimental approaches can be used to analyze the vegetation effect in a woodland. In addition, they can be effectively exploited to the statistical channel model, such as the spatial channel model (SCM) [8]. In [9], microwave and mm-wave propagations in a woodland were studied at 9.6, 28.8, and 57.6 GHz in experiments of one study. Their measurements were conducted under both summer and winter conditions, and the results showed that foliage loss increased rapidly at short foliage depths due to the high attenuation of the main direct path, and a reduced rate of loss was observed at greater depths. In [12], a modified model based on the measurements at 24 GHz was presented from measurements. However, the measurements were conducted for only very short, vegetation depths. In our earlier study [13], channel measurements in vegetated areas at 28 GHz were performed for long foliage depths and we found that excess loss in vegetated areas is associated with a saturating trend with upper-bounded attenuation at 28 GHz.

In this communication, we made extensive foliage measurements at 28 GHz to characterize mm-wave propagation through vegetation as a subsequent study to [13]. For precise classification and analysis of propagation paths, we first propose a pattern matching algorithm and examine it in this communication. The proposed algorithm is one of the high-resolution algorithms and exploits the beam pattern information in the real domain. This method allows us to overcome the angle resolution of a directional antenna and to estimate a more accurate receiving angle. Then the received paths for each measurement point were classified into various propagation components according to the reflectors/scatterers on the estimated receiving angle. The propagation components can be discriminated as leaves, trunks,

Manuscript received October 26, 2017; revised May 19, 2019; accepted October 20, 2019. Date of publication January 30, 2020; date of current version May 5, 2020. *(Corresponding author: Junghoon Ko.)*

Junghoon Ko, Yun-Seok Noh, Dong-Jo Park, and Dong-Ho Cho are with the School of Electrical Engineering, Korea Advanced Institute of Science and Technology (KAIST), Daejeon 34141, South Korea (e-mail: junghoon_ko@kaist.ac.kr).

Sooyoung Hur, Kuyeon Whang, and Jeongho Park are with Samsung Electronics, Suwon 16677, South Korea.

Color versions of one or more of the figures in this communication are available online at http://ieeexplore.ieee.org.

Digital Object Identifier 10.1109/TAP.2020.2968801

ground, walls, and others. We found that a tree clutter (leaves and tree trunks) serves as a main propagation factor compared with other environmental components, such as building walls, ground, and so on. The power ratios for the propagation components were also calculated from the summation of the corresponding powers of the classified paths. In addition, we discuss foliage attenuation models for the mm-wave bands at 28 GHz based on the measurement data. The measured results show that the power attenuation rate decreased as the foliage depth increases, as it is well matched with the results in [13]. Furthermore, the effects of foliage attenuation on seasonal changes were also studied. Finally, channel characteristics including delay spread, coherence bandwidth, and angular spreads were statistically described in vegetated areas.

II. Measurement Campaign

A. Measurement System Description

The 28 GHz propagation measurements were performed using a correlator-based channel sounder which exploited pseudorandom noise (PN) sequences. The chip rate of the PN sequences and the sampling rate of an analog-to-digital converter (ADC) were 250 Mega chip-per-second (Mcps) and one Giga sample-per-second (Gsps), respectively. A function generator was linked through a cable connection to synchronize the two sides by generating a common trigger signal. On the Tx side, an omni-directional antenna with a gain of 9.3 dBi was used. However, on the Rx side, a directional horn antenna of 24.5 dBi gain with 10° half-power beamwidth (HPBW) in both azimuth and elevation planes was installed, and only its vertical polarization was considered. The signal power fed to the Tx antenna was up to 29 dBm and the corresponding maximum measurable path loss was approximately 145 dB when we considered the antenna gains at both the Tx and Rx. On the Rx side, directional measurements were made due to the narrow beamwidth of the Rx antenna. Therefore, antenna scanning was needed in all possible directions in which signals can be received in vegetated areas. Further details about the channel sounder can be found in our earlier work [2].

The process of obtaining a channel power delay profile (PDP) using this measurement system is as follows. As introduced above, the channel sounder obtains a directional channel PDP from a directional antenna on the Rx side. Multiple directional profiles can be aligned in the delay domain by using the time-synchronization technique proposed in [1]. After aligning the PDPs, we finally corrected the receiving angle for each time delay by performing a pattern matching algorithm (Section II-C).

B. Measurement Scenario

The foliage measurement campaign at 28 GHz was performed in urban environments in downtown Daejeon, South Korea. The measurements were conducted in three measurement sites in which the Rx was positioned near a line of trees and the Tx was placed across from the receiver; the first measurement was performed in a park, and the other measurement sites were near the apartment buildings. In general, the environments in which the measurements were carried out were similar to that in a typical urban area with vegetation. Fig. 1 shows the satellite maps of the three measurement sites. The areas selected for the measurements included several types of trees: Korean maple, ginkgo, and Korean pine trees. At all of the measurement locations, the heights of trees (h_f) ranged from 7 to 11 m. The radii of the tree canopies (r_f) were different for each measurement site ranging from 2 to 4 m. The Tx and Rx antennas were installed at heights of 6 and 4 m, respectively. Measurement data were obtained in October 2016, when the trees were with leaves in dry weather conditions. Detailed parameters including the distance

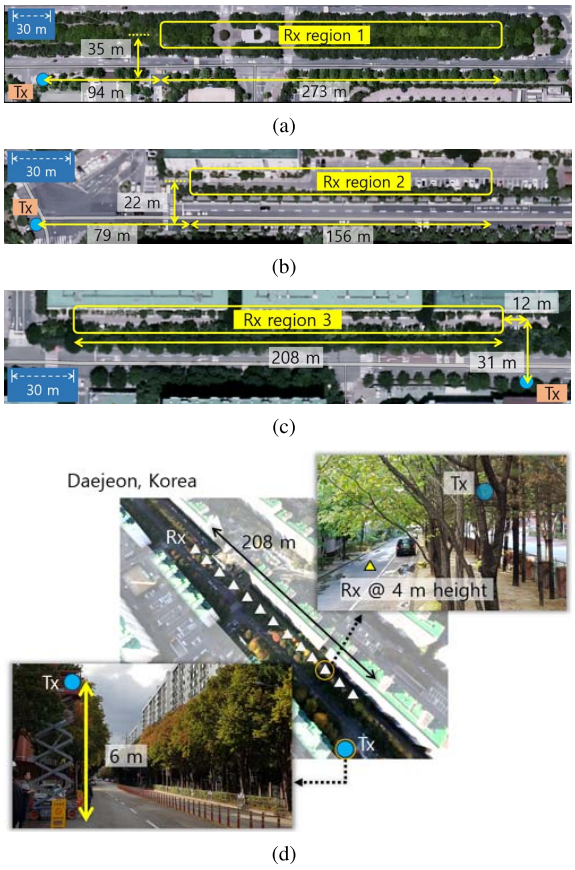

Fig. 1. Satellite maps of the foliage measurement sites: (a) region 1 (park), (b) region 2 (apartment buildings), (c) region 3 (apartment buildings), and (d) example of measurement campaigns in region 3.

TABLE I
Information for the Measurement Locations

Locations	1	2	3
Tx-Rx distance range [m]	100 - 370	80 - 240	30 - 230
Tx/Rx height [m]	6 / 4	6 / 4	6 / 4
Average height of trees [m]	10	9	9
Average radius of canopies [m]	3.5	2.4	3.0
Path discrimination	X	O	O
Foliage attenuation	O	O	O
Seasonal variation	X	X	O

range between the Tx and Rx (d_{tr}) and information on measurement scenarios are listed in Table I. There were three considered scenarios in this communication as follows.

1) Propagation Path Discrimination: In the first measurement scenario, measurements were carried out to discriminate received paths from surrounding buildings and the ground as well as vegetation. This experiment allows us to understand how the signal arrives in the environment where the receiver is surrounded by vegetation and residential buildings. For this scenario, at the Rx regions 2 and 3, the Rx antenna was swept for the azimuth range from −90° to 90° and the elevation range from −30° to 30°. The selected angular steps were 10° in both the azimuth and elevation planes. Therefore, the total number of scanned points at one receiving point is 133 – the number of measurements in the horizontal and elevation planes is 19 and 7, respectively. Note that an omnidirectional antenna was used on the Tx side.

2) Foliage Attenuation: The second scenario focused on the obstructed link between the Tx and Rx antennas by the foliage. Scanning angles at each Rx point were adaptively considered depending

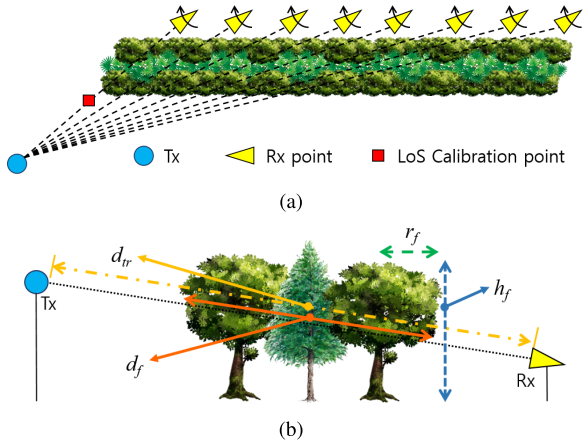

Fig. 2. Overview of measurement scenarios: (a) scenario for foliage attenuation and (b) definitions of distance (d_{tr}) between Tx and Rx, and foliage depth (d_f).

upon the environment of the measurement site. That is, the scanning range of the directional Rx antenna had been determined in order that all the signals scattered and penetrated from the foliage could be captured. In the scanning range, directional measurements were also performed at every 10° over both the azimuth and elevation angles. The setup at the transmitter is the same as in the above scenario. A schematic for this measurement scenario is presented in Fig. 2(a). In Fig. 2(b), the foliage depth d_f is defined as the cumulative length of the Tx–Rx path penetrating the foliage.

3) Seasonal Variation: In order to analyze the difference in foliage attenuation due to seasonal changes, additional experiments were conducted in December 2016 at Rx region 3. All measurement conditions except the state of the trees were set to be equal to the conditions of the measurements in October, including the measurement positions of the Tx and Rx and the scanning range of the Rx antenna. In the case of the Korean pine trees, there was no significant difference according to seasonal changes. However, in the case of Korean maple trees and ginkgo, the leaves in December barely covered the trees and contained little moisture, while the leaves in October were lush.

4) Calibration: Prior to measurements for each location, the free-space LoS-reference powers P_{LoS} were measured by aligning the Tx and Rx antennas to the LoS direction [Fig. 2 (a)]. From these LoS samples, the path loss was calculated as follows:

$$PL_{LoS} = P_{Tx} - P_{LoS} + G_{Tx} + G_{Rx} \text{ [dB]} \quad (1)$$

where P_{Tx} is the transmitted power and G_{Tx} and G_{Rx} are the antenna gains connected in the Tx and Rx sides, respectively. In this communication, the transmitter power and antenna gains, such as $P_{Tx} = 29$ dBm, $G_{Tx} = 9.3$ dBi, and $G_{Rx} = 24.5$ dBi, are considered. Then the path losses were compared with the free-space path loss (FSPL), in order to calibrate the channel sounder system. From comparison, we found that the path losses for measured LoS samples were well matched with the FSPL.

C. Pattern Matching Algorithm

Since directional measurements were performed at every 10° on the Rx side, as stated in Section II-B, the angular resolution of the measurement data was limited to 10°. Therefore, it was necessary to correct the receiving angles of the propagation path and their power values for more accurate analysis. In particular, it was important to precisely detect the incident angle in classifying each propagation path, such as scattered and penetrated paths from trees, reflected paths from the surrounding buildings, and reflected paths from the ground. In this communication, we propose a pattern matching

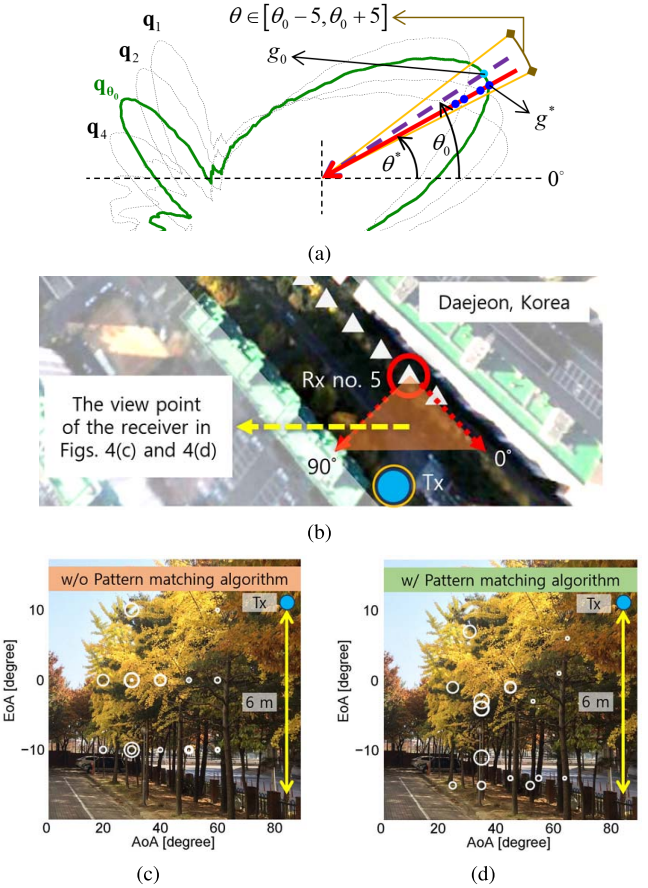

Fig. 3. (a) Principle of the proposed pattern matching algorithm, (b) locations of the receiver and transmitter in region 3, measurement results at Rx no. 5 in region 3: (c) without and (d) with the pattern matching algorithm.

algorithm using the beam pattern information of the (directional) antenna, which was obtained at each 1° interval in both azimuth and elevation angles by the preliminary measurement. We arranged the beam patterns of the directional antenna in the form of a circular array of 10° intervals, so that it would be equivalent to the actual measurement situation through rotation. Then the receiving angle of a path in the two dimension can be more accurately estimated while comparing the received power vector with the equivalent antenna beam pattern vector. Here the considered pattern matching algorithm basically assumed that only one signal comes in during one measuring time. In other words, we assumed that only one signal is received within 1 ns (the sampling rate = 1 Gsps) for the measured data through the channel sounder used in this communication. Note that there has not yet been published a communication improving the accuracy of direction of paths exploiting angle estimation algorithms for directional measurement systems, while the well-known high-resolution algorithms such as SAGE [14] have been used for the omnidirectional channel sounder in the mm-wave bands.

Fig. 3(a) shows the principle of the proposed algorithm. For the sake of simplicity and without the loss of generality, we restricted the following estimation example to the case of 1-D angle. When a path is received at θ^* degrees through the antenna gain of g^* (a solid red line) at a propagation time delay τ, the receiving angle and the corresponding antenna gain are considered as θ_0 degrees and the antenna gain of g_0 (a broken violet line) due to the limitation of the angular resolution (from scanning in 10° increment). Applying the pattern matching algorithm, it is possible to estimate the incident angle of the received signal with a resolution of 1°, by comparing the measured power vector (10° interval) with the known beam

pattern information (1° interval). For better understanding, there is an example as follows: Suppose a signal is coming at an angle of 2°. The signal is also detected in measurements around that angle; 2 ± 10, 2 ± 20, ... Here these duplicated signals are received with different received power values because different antenna gains are applied according to the directional angles of the antennas in each of the directional measurements; this received power vector is defined as $\mathbf{p}$.

However, due to the limitation of the angular resolution, we consider that the signal comes in a 0° and the corresponding adjacent angles; 0 ± 10, 0 ± 20, ... On the other hand, we can obtain a pattern vector from the beam pattern values at a certain direction and the corresponding angles with 10° intervals, because the beam pattern information of the antenna can be known in advance through the preliminary measurements; q_θ, $q_{\theta\pm10}$, $q_{\theta\pm20}$, ... and $\theta = 0, 1, \ldots, 359$. Then by comparing some candidate groups of these pattern vectors (q_θ, $q_{\theta\pm10}$, $q_{\theta\pm20}$, ... and $\theta = 0, \pm1, \ldots, \pm5$) with the power vector $\mathbf{p}$, a more precise receiving angle can be estimated and the angular resolution of the horn antenna can be enhanced. In order to express the process mathematically, we need the following definitions: N_{Rx} is the number of directional measurements at the Rx, k is index of the directional measurements ($1 \le k \le N_{Rx}$), ϕ_k and p_k are the kth Rx pointing angle, and the corresponding power value, respectively. Here the angular spacing between ϕ_{k-1} and ϕ_k is related to the rotating angular steps and is 10° for our measurements. The received power vector $\mathbf{p}$ which has the unit of power from directional measurements can be written as

$$\mathbf{p} = [p_1, \ldots, p_k, \ldots, p_{N_{Rx}}]^T \in \Re^{N_{Rx}\times 1} \tag{2}$$

where $[\cdot]^T$ denotes the transpose.

From the antenna pattern value q_l obtained by preliminary measurements at each 1° interval ($0 \le l \le 359$), we can also obtain a pattern vector $\mathbf{q}$ and a shifting vector $\mathbf{q_k}$ which is computed by circularly shifting $\mathbf{q}$ by ϕ_k given as

$$\mathbf{q} = [q_0, q_1, \ldots, q_l, \ldots, q_{359}]^T \in \Re^{360\times 1} \tag{3}$$

$$\mathbf{q_k} = [q_{-\phi_k}, q_{1-\phi_k}, \ldots, q_{l-\phi_k}, \ldots, q_{359-\phi_k}]^T \in \Re^{360\times 1}. \tag{4}$$

Note that the dimension of the shifting vector $\mathbf{q_k}$ is equal to those of the pattern vector $\mathbf{q}$. Then we can define a matrix $\mathbf{Q}$ as follows:

$$\mathbf{Q} = \begin{bmatrix} \mathbf{q}_1^T \\ \mathbf{q}_2^T \\ \vdots \\ \mathbf{q}_{N_{Rx}}^T \end{bmatrix} = [\hat{\mathbf{q}}_0, \ldots, \hat{\mathbf{q}}_\theta, \ldots, \hat{\mathbf{q}}_{359}] \in \Re^{N_{Rx}\times 360} \tag{5}$$

where $\hat{\mathbf{q}}_\theta$ is the θth column vector of the matrix $\mathbf{Q}$ ($0 \le \theta \le 359$), whose dimensions are $N_{Rx} \times 1$. Finally, the optimum receiving angle θ^* can be estimated by the following equation:

$$\theta^* = \arg\min_\theta \|\mathbf{p} - \alpha_\theta \hat{\mathbf{q}}_\theta\|^2, \quad \theta \in [\theta_0 - 5, \theta_0 + 5] \tag{6}$$

where

$$\alpha_\theta \triangleq \frac{\hat{\mathbf{q}}_\theta^T \mathbf{p}}{\|\hat{\mathbf{q}}_\theta\| \|\mathbf{p}\|}. \tag{7}$$

Here α_θ is a unitless scaling factor. If the optimal receiving angle is accurately estimated, then $\hat{\mathbf{q}}_{\theta^*}$ includes the blue points (on the red arrow) in Fig. 3(a). The antenna gain under consideration also changes from g_0 to g^*, leading to a correction of the path loss.

Fig. 3(b)–(d) shows the measured results obtained at a specific Rx point in region 3. For 2-D angular regions , the figure shows an unprocessed result and a processed result with the pattern matching algorithm, with photographs of the corresponding position in Fig. 3(c) and (d), respectively. The white circles represent each of the receiving paths, and the size of the circle represents the intensity (power) of the signal: the greater the size of the circle, the greater the intensity of the signal. As Fig. 3 reveals, the proposed pattern matching algorithm allows us more precise discrimination of multiple paths by estimating a finer receiving angle.

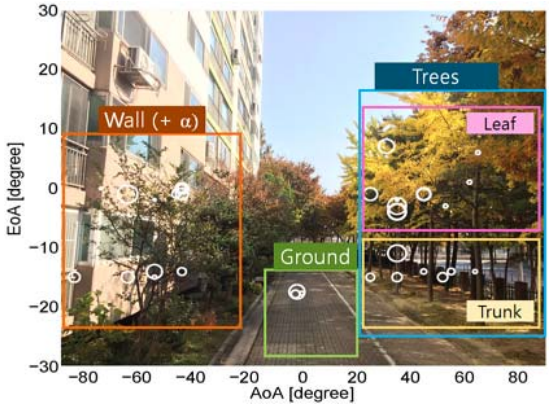

Fig. 4. Example of discriminating propagation paths based on measurement data at Rx no. 5 in region 3 (the view point of the receiver).

TABLE II
POWER RATIOS OF THE PROPAGATION PATHS

Scatterers	Trees		Building Walls (+ α)	Ground	Etc.
	Leaves	Trunks			
Regions 2 & 3	41.49	17.62	24.53	6.37	9.99

III. MEASUREMENT RESULTS AND ANALYSIS

A. Propagation Path Discrimination

In residential areas with vegetation such as regions 2 and 3 in Fig. 1, there are several paths from building and ground reflections as well as paths from tree clutters. In this section, propagation paths were discriminated and the power ratio of each path was analyzed. The received paths for each measurement point in regions 2 and 3 were classified into various propagation components according to the reflectors/scatterers on the received angle. The propagation components can be divided into scattering paths from trees, reflection paths from the ground, reflection paths from buildings, and other paths as shown in Fig. 4. The scattering paths from the tree clutters were analyzed by further dividing them into penetration paths by leaves and reflection paths by tree trunks. Note that the reflection paths from buildings suffered additional losses through vegetation due to the environment of the measuring point. Then the power and power ratios for each propagation component were calculated from the summation of the corresponding powers of the classified paths. Finally, Table II shows an average of the power ratios for propagation components obtained from all the measurement locations in regions 2 and 3. The result shows that tree clutter plays a role of the strongest cluster and the walls of buildings make up the second valid cluster. The effect of ground reflection was not much greater than expected, because the condition of the ground plane at the receiving point is not flat but bumpy. In the case of the tree clutter, the paths from the leaves had a little more energy than the paths from the tree trunks.

In addition, these measurements give us a notable insight. In the case of signals received through the vegetation, it was observed that not only the transmitted (penetrated) path but also diffusive components were received. This means that the received signal contains several noncoherent diffusive components as well as a coherent component with a well-defined direction. Therefore, the foliage attenuation of the signal according to the foliage depth does not

continuously increase and saturates, and it becomes more apparent when considering the signals from the surrounding environments such as buildings or the ground. Foliage attenuation showing this analysis were presented and discussed in Section III-B.

B. Foliage Attenuation

From the obtained PDPs, we defined two kinds of received powers. First, we considered the strongest power component $P_{\max}$ measured at a specific time delay through a single beam of 10° beamwidth. In addition, when a rich-scattering environment is exploited in vegetated areas, a beam combining gain can be evaluated by using multiple beams with adaptive antenna systems. In this communication, we used the combined power sample P_{sum} resulting from the noncoherent sum of the three strongest power components. The comparison results of two types of powers show that spatial multipath could be exploited to achieve average gains of approximately 2.4 dB. Then it was possible to calculate the foliage attenuations for each measurement point from the received powers as indicated in the following equation:

$$\begin{cases} L_{f,\max} = P_{LoS} - P_{\max} \text{ [dB]} \\ L_{f,sum} = P_{LoS} - P_{sum} \text{ [dB]}. \end{cases} \tag{8}$$

There are two commonly used models that represent the degree of foliage attenuation over distance. The first one is the modified exponential decay (MED) model, which was used in [10] and [13]. This model is also introduced for slant path propagations in [11] and has three parameters as shown in the following equation:

$$L_f = a \cdot f^b \cdot {d_f}^c \text{ [dB]}. \tag{9}$$

Here f is the frequency in megahertz and d_f is the foliage depth in meters. The parameters for the above two models were estimated to fit a measurement data set according to the minimum root-mean-square (rms) criterion. In this communication, the center frequency f was set to 28 GHz and the foliage depth d_f was calculated at each Rx point. An alternative approach is the maximum attenuation (MA) model, which is recommended for a terrestrial radio path in woodland in ITU-R Recommendation P.833-8 [11] as follows:

$$L_f = A_m \cdot \left(1 - \exp\left(-\frac{\gamma}{A_m} d_f\right)\right) \text{ [dB]}. \tag{10}$$

The model parameters γ and A_m indicate a specific attenuation for very short paths and the MA, respectively. This model was also considered in [12] and [13].

Scatter plots of the foliage attenuation are shown with the two models in Fig. 5. As expected in (9) and (10), the attenuation rate in the vegetated areas (the slope of the models) decreases with the foliage depth. The foliage attenuation tends to converge as the foliage depth becomes deeper. The prediction errors between the measurements and the two models were quantified by finding the mean absolute error (MAE), the root-mean-squared error (RMSE) and their relative errors given as follows:

$$\text{MAE} = \frac{1}{N}\sum_{i=1}^{N}|x_i - a_i|, \quad \text{RAE} = \frac{\sum_{i=1}^{N}|x_i - a_i|}{\sum_{i=1}^{N}|\bar{a} - a_i|} \tag{11}$$

$$\text{RMSE} = \sqrt{\frac{1}{N}\sum_{i=1}^{N}(x_i - a_i)^2}, \quad \text{RSE} = \frac{\sum_{i=1}^{N}(x_i - a_i)^2}{\sum_{i=1}^{N}(\bar{a} - a_i)^2} \tag{12}$$

where N is the total number of measurement points, a_i and x_i are the actual and predicted values at the ith measurement point.

The mean value of measurement vector elements is denoted as $\bar{a}$, and the RAE and RSE indicate the relative absolute error and relative squared error, respectively. Table III shows the quantified error values for both the MED and MA models. From the MA model, the MA value in the vegetation area is roughly determined and a system designer could take advantage of these values when planning out a network. However, it was confirmed that the MED model describes the measurement results more accurately in a least squares perspective (Fig. 6). The MA values in the MA model were approximately 40 dB, and the difference between both the received powers ($P_{\max}$ and P_{sum}) was about 2 dB. It means that the coherent component with the well-defined propagation direction is decreased due to both absorption and scattering, and its decay rate is high. However, the noncoherent component is attenuated due to absorption only and has relatively slower attenuation rate. The coherent component dominates at short foliage depth leading to a high attenuation rate, whereas the diffuse component becomes dominant at large vegetation depths.

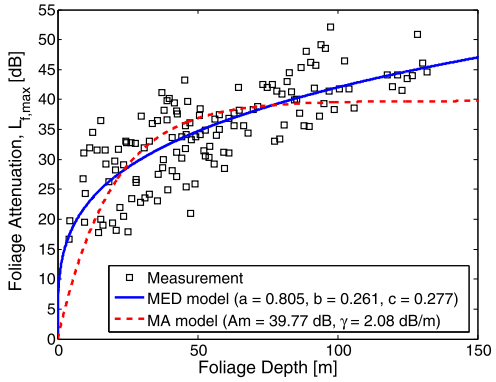

(a)

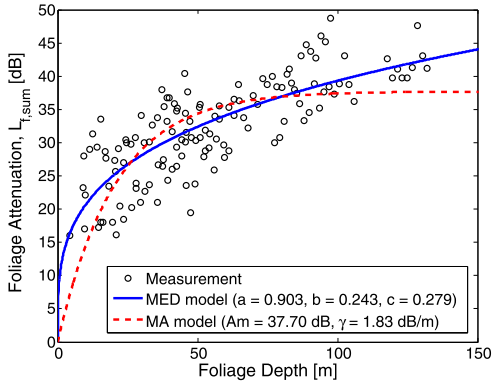

(b)

Fig. 5. Measured and modeled foliage attenuation: (a) for $P_{\max}$ and (b) for P_{sum}.

TABLE III
ERRORS BETWEEN MEASUREMENTS AND PREDICTION MODELS

Reference Power	Prediction Model	Prediction Errors			
		MAE	RMSE	RAE	RSE
$P_{\max}$	MED [dB]	4.1051	5.0301	0.6483	0.4125
	MA [dB]	5.0382	6.2454	0.7956	0.6359
P_{sum}	MED [dB]	3.7562	4.5570	0.6277	0.3889
	MA [dB]	4.4993	5.6197	0.7518	0.5914

C. Seasonal Variation

The difference in foliage attenuation resulting from seasonal variations was observed by measuring at the same positions in region 3 in October and December 2016. In Fig. 6, the excess losses due to foliage for the two seasons were compared according to

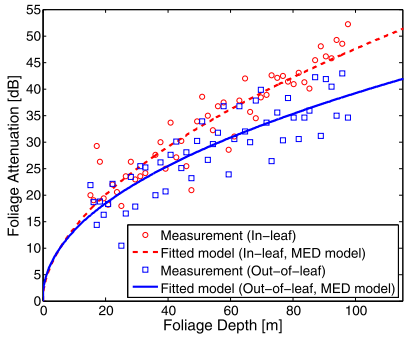

Fig. 6. Comparison of the foliage attenuation results for seasonal changes.

TABLE IV

MEAN VALUES OF WIDEBAND CHANNEL PARAMETERS FOR PROPAGATION CHANNELS BY SOME SCATTERERS

	Tree Leaves	Tree Trunks	Building Walls	Ground
Delay Spread	40.18ns	31.67ns	23.32ns	17.01ns
Coherence BW	45.58MHz	47.39MHz	99.38MHz	105.18MHz
Azimuth AS	13.55deg	15.01deg	12.84deg	4.58deg
Elevation AS	5.20deg	2.73deg	7.50deg	3.28deg

the foliage depth. Here the foliage depth and the received powers were considered based on the leafy environment in October and the strongest power sample P_{max}, respectively. The result indicated that there was an attenuation reduction of about 10 dB at a depth of 100 m in the leafless season compared with the leafy season.

D. Spatiotemporal Channel Characteristics

We analyzed the channel properties in terms of delay spread (S_τ), coherence bandwidth (S_f), and angular spreads (AS, S_ψ), on the basis of the estimated omnisynthesized PDPs (P_τ) and power angular spectrums (P_ψ) [1], [15]. Table IV shows the mean values of these parameters from each of the propagation channels by tree leaves, tree trunks, building walls, and ground. The propagation channels scattered from the tree leaves were most dispersed in the time and angular domains, while the propagation channels reflected from the ground has the most concentrated property. In other words, the coherence region in the frequency was wider in the ground/wall-reflected channel than the scattered propagation channel by tree clutters. Note that all the channel parameters in the following equations follow the log-normal distribution well

$$S_\tau = \sqrt{\frac{\int_\tau P_\tau(\tau)\tau^2 d\tau}{\int_\tau P_\tau(\tau)d\tau} - \left(\frac{\int_\tau P_\tau(\tau)\tau d\tau}{\int_\tau P_\tau(\tau)d\tau}\right)^2}, \quad S_f = \frac{1}{S_\tau} \tag{13}$$

and

$$S_\psi = \sqrt{\frac{\int_\psi |e^{j\psi} - M_\psi|^2 P_\psi(\psi)d\psi}{\int_\psi P_\psi(\psi)d\psi}} \tag{14}$$

where

$$M_\psi = \frac{\int_\psi e^{j\psi} P_\psi(\psi)d\psi}{\int_\psi P_\psi(\psi)d\psi}. \tag{15}$$

IV. CONCLUSION

In this communication, foliage measurements at 28 GHz were performed using a directional channel sounder for typical urban residential areas in Daejeon, South Korea. For precise classification and analysis of propagation paths, a pattern matching algorithm was proposed that allows us to overcome the angle resolution of a directional antenna and to estimate a more accurate receiving angle. Propagation paths received from the vegetation and the surrounding buildings were discriminated and analyzed with their power ratios. It was found that tree clutters are the strongest cluster and the walls of buildings are the second valid cluster. The effect of ground reflection was not much greater than expected. In addition, foliage attenuations were analyzed and appropriate models were presented based on the MED model and the MA model. Two types of received powers were considered for calculating excess loss in foliage areas, which include the strongest power component, P_{max}, and the combined power sample, P_{sum}. The comparison results of the two types of powers showed that the spatial multipath could be exploited to achieve average gains of approximately 2.4 dB. The effect of foliage attenuation on seasonal changes was further studied. About a 10 dB reduction in foliage attenuation was found at a depth of 100 m in the leafless environment compared with the leafy one. Finally, statistical properties in the vegetated channel were analyzed in typical residential environments. By using our proposed algorithm, detailed propagation channels were identified and analyzed based on the wideband channel parameters. The measured result indicates that the scattered channel from the tree shows the most dispersed characteristics in both the time and space domains.

REFERENCES

[1] S. Hur, Y.-J. Cho, J. Lee, N.-G. Kang, J. Park, and H. Benn, "Synchronous channel sounder using horn antenna and indoor measurements on 28 GHz," in *Proc. IEEE Int. Black Sea Conf. Commun. Netw. (BlackSeaCom)*, May 2014, pp. 83–87.

[2] J. Ko *et al.*, "Feasibility study and spatial–temporal characteristics analysis for 28 GHz outdoor wireless channel modelling," *IET Commun.*, vol. 10, no. 17, pp. 2352–2362, Nov. 2016.

[3] J. Ko *et al.*, "Millimeter-wave channel measurements and analysis for statistical spatial channel model in in-building and urban environments at 28 GHz," *IEEE Trans. Wireless Commun.*, vol. 16, no. 9, pp. 5853–5868, Sep. 2017.

[4] T. S. Rappaport, R. W. Heath, Jr., R. C. Daniels, and J. N. Murdock, *Millimeter Wave Wireless Communications*, 1st ed. Upper Saddle River, NJ, USA: Prentice-Hall, 2015.

[5] D. Didascalou, M. Younis, and W. Wiesbeck, "Millimeter-wave scattering and attenuation in limited vegetation structures," in *Proc. Int. Conf. Geosci. Remote Sens. Symp.*, Jul. 1999, pp. 1835–1838.

[6] F. Mani and C. Oestges, "A ray based method to evaluate scattering by vegetation elements," *IEEE Trans. Antennas Propag.*, vol. 60, no. 8, pp. 4006–4009, Aug. 2012.

[7] N. R. Leonor, R. F. S. Caldeirinha, T. R. Fernandes, D. Ferreira, and M. Sánchez, "A 2D tay-tracing based model for micro- and millimeter-Wave propagation through vegetation," *IEEE Trans. Antennas Propag.*, vol. 62, no. 12, pp. 6443–6453, Dec. 2014.

[8] *Study on 3D Channel Model for LTE (Relaease 12)*, document TR 36.873 V12.7.0, 3GPP, Dec. 2017.

[9] F. Schwering, E. Violette, and R. Espeland, "Millimeter-wave propagation in vegetation: Experiments and theory," *IEEE Trans. Geosci. Remote Sens.*, vol. GRS-26, no. 3, pp. 355–367, May 1988.

[10] M. Al-Nuaimi and R. Stephens, "Measurements and prediction model optimisation for signal attenuation in vegetation media at centimetre wave frequencies," *IEE Proc., Microw. Antennas Propag.*, vol. 145, no. 3, pp. 201–206, 1998.

[11] *Attenuation in Vegetation*, document Rec. ITU-R P.833-8, Sep. 2013.

[12] I. Rodriguez, R. Abreu, E. P. L. Almeida, M. Lauridsen, A. Loureiro, and P. Mogensen, "24 GHz cmwave radio propagation through vegetation: Suburban tree clutter attenuation," in *Proc. 10th Eur. Conf. Antennas Propag. (EuCAP)*, Apr. 2016, pp. 10–15.

[13] J. Ko *et al.*, "28 GHz millimeter-wave measurements and models for signal attenuation in vegetated areas," in *Proc. 11th Eur. Conf. Antennas Propag. (EUCAP)*, Mar. 2017, pp. 1808–1812.

[14] J. Fessler and A. Hero, "Space-alternating generalized expectation-maximization algorithm," *IEEE Trans. Signal Process.*, vol. 42, no. 10, pp. 2664–2677, Oct. 1994.

[15] J. Ko, "Characteristics analysis and modeling of millimeter-wave propagation channel based on 28 GHz channel measurements," Ph.D. dissertation, Korea Adv. Inst. Sci. Technol. (KAIST), Daejeon, South Korea, Feb. 2018.